Optimization of methanol synthesis reaction on Cu/ZnO/Al₂O₃/ZrO₂ catalyst using genetic algorithm: Maximization of the synergetic effect by the optimal CO₂ fraction

Hye-Won Lim*, Hye Jin Jun*, Myung-June Park*,†, Hyo-Sik Kim**, Jong Wook Bae**,
Kyoung-Su Ha**, Ho-Jeong Chae**, and Ki-Won Jun**

*Department of Chemical Engineering, Ajou University, Suwon 443-749, Korea
**Petroleum Displacement Technology Research Center, Korea Research Institute of Chemical Technology (KRICT),
Daejeon 305-600, Korea

Abstract−A kinetics model that takes the synergetic effect of carbon dioxide fraction on the methanol production rate into account is applied to the development of a mathematical model for the bench-scale reactor. A comparison between the simulation results and the experimental data corroborates the validity of the model. Several optimization strategies are suggested to maximize the methanol yield, among which the utilization of piecewise trajectories for wall temperature along the reactor axis as well as the optimal CO₂ fraction at the inlet of the reactor is found to be the best strategy in the sense of methanol production per unit amount of the feed, in such a way that the optimization strategy considers the variation of the reaction temperature in the reactor and maximizes the synergetic effect on the production rate by the addition of carbon dioxide.

Key words: Methanol, Mathematical Model, Bench-scale Reactor, Cu-based Catalyst, Optimization, CO₂ Fraction

INTRODUCTION

Methanol is known to be an excellent fuel in its own right that can be conveniently converted into ethylene or propylene in the methanol-to-olefins (MTO) process. In turn, these olefins can be used to produce hydrocarbon fuels and their products [1,2]. Methanol is also used as intermediate material for the production of many useful chemicals such as formaldehyde, acetic acid and so on, and it has been recently reported that methanol can be used in the direct methanol fuel cell (DMFC) [3]. Methanol is synthesized via CO and CO₂ hydrogenation, and since the advent of the first commercial process developed by BASF in 1923 using ZnO-Cr₂O₃ catalyst [4], many research works have focused on the commercialization of methanol synthesis. In addition, it is known that production rate and energy cost of large-scale processes can be effectively optimized through the manipulation of several operation variables.

Methanol synthesis is classified into two categories: low pressure and high pressure processes. In high pressure processes, the typical catalyst is ZnO-Cr₂O₃ and the pressure and the temperature ranges are from 24 to 30 MPa and 350-400 °C, respectively. Meanwhile, low pressure processes operate within a pressure of 5-10 MPa and temperature of 240-270 °C, respectively, since a temperature higher than 270 °C results in the deactivation of the catalyst due to the sintering problem. Although Cu/ZnO/Al₂O₃ catalyst is easily poisoned by sulfur, it is used in low pressure processes since persistent studies have shown that alumina-based catalysts had better catalytic activity and longer-term stability compared to the utilization of chromia as a promoter. The mechanism for these alumina-based catalysts is similar to that of low temperature water-gas shift catalysts

but differs in detailed formulation. Another benefit of low pressure processes is less formation of by-products. All in all, the operation under low pressure and low temperature corresponds to the reduction of operating cost, and thus, Cu/ZnO catalyst is widely used in most methanol synthesis processes [5].

Although many kinetic mechanisms have been suggested for the synthesis of methanol and water, the exact mechanism is not clearly discussed. Herman and coworkers [6] proposed a dual site mechanism for the dissociative adsorption of hydrogen molecule on the ZnO while carbon monoxide is adsorbed on the site of monovalent copper. Similarly, the kinetics for the synthesis of methanol from carbon dioxide by a Cu-based catalyst was reported more than two decades ago [7,8]. According to the reports, the kinetic mechanism for the methanol synthesis may involve both CO and CO₂. Klier and coworkers [9] assumed the adsorption of reactants and they evaluated the effect of carbon dioxide on the catalytic synthesis of methanol over the copper-zinc oxide catalysts. They also proposed several mechanisms: (1) H₂, CO, and CO₂ were assumed to adsorb on the catalyst competitively (single site mechanism), (2) CO and CO₂ were assumed to adsorb on the catalyst competitively while hydrogen adsorbs on the different site from CO and CO₂ (dual site mechanism), (3) the adsorption sites for CO and H₂ are different and CO₂ competes for both the CO sites and the hydrogen sites. For more detailed elementary steps, it was shown that carbon monoxide is adsorbed in the form of a carbonyl species, and a formate species is a usual intermediate for methanol synthesis and water gas shift reaction [10]. There are many reports introducing the adsorption of CO and CO₂ on two different sites [9,11,12]. However, since their work ignores the water-gas-shift (WGS) reaction, the relationship between CO and CO₂ (e.g., synergetic effect of CO₂) on the methanol synthesis reaction rate is not clearly understood. Recently, Lim and coworkers [13] developed a kinetics model on

the basis of different sites on Cu for the adsorption of carbon monoxide and carbon dioxide, and they showed that a small fraction of carbon dioxide accelerates the production of methanol indirectly via WGS reaction.

Because of severe temperature effects, an optimal temperature policy is a key to the optimal operation of a methanol synthesis reactor. Løvik and coworkers [14] studied dynamic modeling and optimization of a methanol synthesis reactor, including the estimation of a catalyst deactivation model, while other researchers showed that the optimal reactor with two-stage cooling shell presented higher performance [15,16]. Recently, Rahimpour and Elekaei Behjatia [17] proposed two-step optimization approaches to maximize the methanol production rate. In their first approach, the optimal temperature profile along the reactor was studied and then, a stepwise approach was followed to determine the optimal profiles for saturated water and gas temperatures in three steps during the operation.

However, in spite of many reports involved with the optimization of methanol synthesis reactor, little effort has focused on the effect of CO_2 fraction as a function of temperature on the maximum methanol production rate. Therefore, in the present study, the kinetics model developed in our previous work [13] is used to evaluate the role of CO_2 fraction to the methanol yield, and then, an optimization strategy is suggested to utilize the fraction as well as temperature profile for the development of the most efficient methanol synthesis reactor.

EXPERIMENTAL

1. Catalyst Preparation and Activation

The catalyst was prepared by co-precipitation method using an aqueous solution containing copper acetate, zinc acetate, aluminum nitrate and zirconium oxide nitrate of required quantities (weight ratio of CuO/ZnO/Al₂O₃/ZrO₂=61.5/31.5/3.3/3.7). The precipitant, Na_2CO_3, was dissolved in deionized water and two separate solutions of precipitant and metal precursors were simultaneously precipitated with a controlled feeding rate of 200 mL/min at 343 K at a severe stirring condition. The final pH of the solution was maintained at around 7. The precipitate was further aged for 3 h at 343 K and then washed several times with deionized water. The dried power was calcined at 573 K for 5 h. The calcined powder was pelletized to form a cylindrical pellet in a size of 5×3 mm (diameter x length). Catalytic activity tests were carried out in a tubular fixed bed reactor (38 mm of inner diameter with a length of 500 mm) with a pellet-type catalyst weight of 350 g and a catalyst-bed height of 324 mm. Prior to reaction, the methanol synthesis catalyst was reduced for 12 h at 523 K under flow of 5% H_2 balanced with nitrogen gas.

2. Bench-scale Reactor and Activity Test

The synthesis gas was produced by using a mixed steam and carbon dioxide reforming of methane (SCR) reaction to adjust an appropriate H_2/CO ratio for methanol synthesis reaction. The feed molar composition of $CH_4/H_2O/CO_2$ was adjusted to 1/1.5/0.39 at steady-state by controlling CH_4 and CO_2 conversion at around 93 and 57% at the reaction conditions of T=1,123 K (average temperature in catalyst-bed), P=0.65 MPa and space velocity (SV)=1,700 ml-CH_4/gcat/h. The molar ratio of produced synthesis gas from SCR reaction was found to be around 0.87 and 0.93 of $CO/(CO+CO_2)$ and $H_2/(2CO+3CO_2)$, respectively. For methanol synthesis, a double-jacketed reactor equipped with an oil circulator to remove the heat of reaction was adopted in the present investigation. See Fig. 1 and Table 1 for a schematic diagram and specifications of reactors for
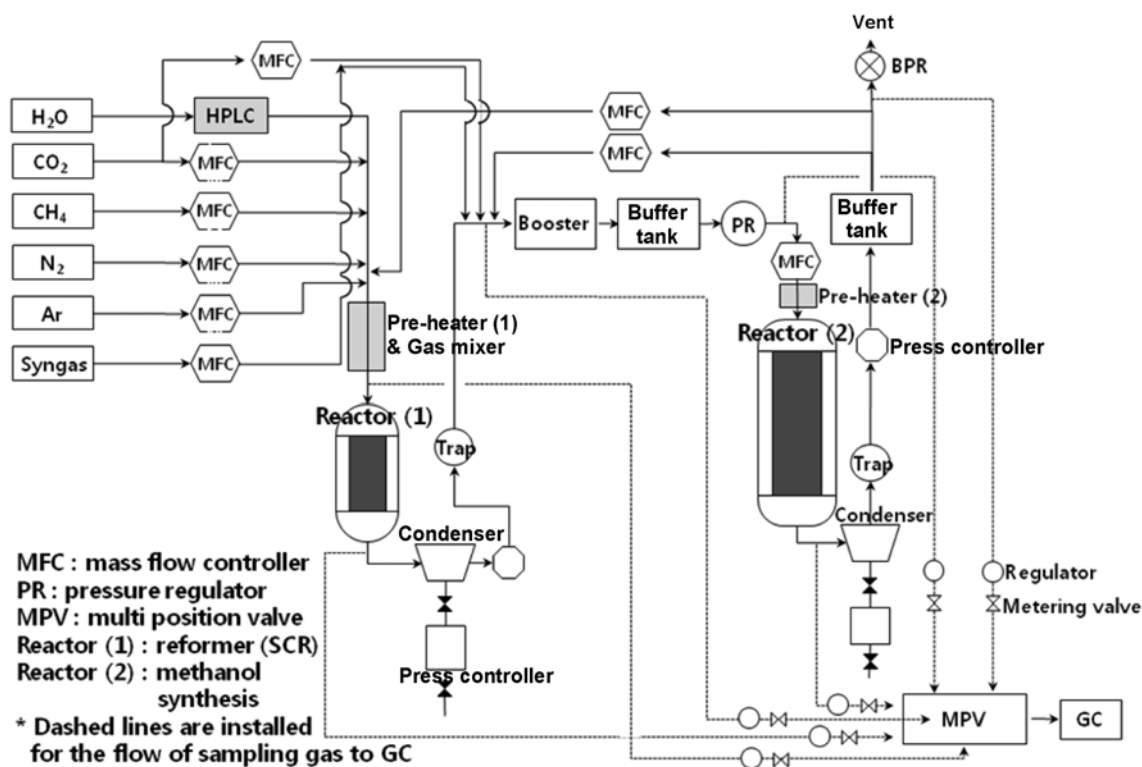

Fig. 1. Schematic diagram of the bench-scale reactor.

Table 1. Physical properties and reactor specification

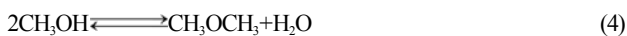| Parameter	Value	Unit
Bulk gas density (ρ_g)	14.38	kg/m^3
Bulk pellet density (ρ_B)	952	kg/m^3
Catalyst weight	0.35	kg
Tube diameter (D)	3.8	cm

SCR and methanol synthesis reaction with a recycling system of unreacted synthesis gas and multi-position sampling points of effluent gas.

As shown in Fig. 1, the unreacted synthesis gas was recycled to a methanol synthesis reactor and the reaction was carried out at the reaction conditions of T (oil circulator)=523 K, P=5.0 MPa and SV=4,700 ml/gcat/h. The feed molar composition at the inlet of methanol synthesis reactor at steady-state with a recycle of unreacted synthesis gas was found to be around 0.72 for CO/(CO+CO$_2$) with a molar ratio of H$_2$/CO/CO$_2$=2.84/1/0.39. The CO conversion at steady-state after 10 h on stream without showing a significant catalyst deactivation was selected to carry out further reactor modeling. The products were analyzed by using an on-line gas chromatograph (YoungLin 6100) equipped with thermal conductivity detector to analyze Ar, CO and CO$_2$ connected with a carbosphere packed column and flame ionized detector for MeOH and hydrocarbons with a GS-Q capillary column.

MATHEMATICAL MODELING

1. Kinetic Mechanism and Reaction Rates

The methanol synthesis reaction is composed of three main reactions: (1) the hydrogenation of carbon monoxide, (2) reversible water gas shift reaction, and (3) the hydrogenation of carbon dioxide. In addition, a side reaction for the synthesis of dimethyl ether (DME) from methanol is considered:

$$CO+2H_2 \rightleftharpoons CH_3OH \tag{1}$$

$$CO_2+H_2 \rightleftharpoons CO+H_2O \tag{2}$$

$$CO_2+3H_2 \rightleftharpoons CH_3OH+H_2O \tag{3}$$

$$2CH_3OH \rightleftharpoons CH_3OCH_3+H_2O \tag{4}$$

Equilibrium constants, K_{PA}, K_{PB}, and K_{PC} for CO hydrogenation (A), reverse WGS reaction (B), and CO$_2$ hydrogenation (C), respectively, are determined by fitting the experimental given in Graaf et al.'s work [18], and the expression for DME production is available in the literature [19] as follows:

$$\ln K_{PA} = \frac{9.8438 \times 10^4}{RT} - 29.07 \tag{5}$$

$$\ln K_{PB} = \frac{-4.3939 \times 10^4}{RT} + 5.639 \tag{6}$$

$$K_{PC} = K_{PA} \times K_{PB} \tag{7}$$

$$K_{P,DME} = 0.106 \exp\left(\frac{2.1858 \times 10^4}{RT}\right) \tag{8}$$

where R represents the gas constant in J/mol/K.

Reaction rate expressions for methanol production have been developed on the basis of a detailed kinetic mechanism and the rate determining step determined by the optimization procedure [13], while the rate of DME production has been determined by other researchers [20]:

$$r_A = \frac{k_A K_{CO} K_{H_2}^2 K_{CH,CO}(P_{CO}P_{H_2}^2 - P_{CH_3OH}/K_{PA})}{(1+K_{CO}P_{CO})(1+K_{H_2}^{0.5}P_{H_2}^{0.5} + K_{H_2O}P_{H_2O})} \tag{9}$$

$$r_B = \frac{k_B K_{CO_2} K_{H_2}^{0.5}(P_{CO_2}P_{H_2} - P_{CO}P_{H_2O}/K_{PB})/P_{H_2}^{0.5}}{(1+K_{H_2}^{0.5}P_{H_2}^{0.5} + K_{H_2O}P_{H_2O})(1+K_{CO_2}P_{CO_2})} \tag{10}$$

$$r_C = \frac{k_C K_{CO_2} K_{H_2} K_{CH,CO_2}(P_{CO_2}P_{H_2}^3 - P_{CH_3OH}P_{H_2O}/K_{PC})/P_{H_2}^2}{(1+K_{H_2}^{0.5}P_{H_2}^{0.5} + K_{H_2O}P_{H_2O})(1+K_{CO_2}P_{CO_2})} \tag{11}$$

$$r_{DME} = \frac{k_{DME} K_{CH_3OH}^2(C_{CH_3OH}^2 - ((C_{H_2O}C_{DME})/K_{P,DME}))}{(1+2\sqrt{K_{CH,OH}C_{CH_3OH}} + K_{H_2O,DME}C_{H_2O})^4} \tag{12}$$

The reaction rate constants and adsorption equilibrium constants which occur in the formulation of kinetic expressions are in Table 2.

2. Reactor Model

Since the L-to-D ratio of the reactor (about 12) used in the experiment is relatively high, radial dispersion is assumed to be negligible, and thus, a one-dimensional model is used. The following equations, considering the gradient between solid and fluid phases, are applied for the mass and energy balances of the fluid phase and catalyst particle [15,21]:

i) For fluid phase

Table 2. Kinetic parameters used in the rate expressions

Kinetic parameters	References
$k_A = 1.16 \times 10^{-9} \exp\left[-\dfrac{7.01 \times 10^3}{R}\left(\dfrac{1}{T} - \dfrac{1}{523}\right)\right]$	Lim et al. [13]
$k_B = 2.82 \times 10^{-5} \exp\left[-\dfrac{2.70 \times 10^2}{R}\left(\dfrac{1}{T} - \dfrac{1}{523}\right)\right]$	
$k_C = 1.15 \times 10^{-6} \exp\left[-\dfrac{1.19 \times 10^2}{R}\left(\dfrac{1}{T} - \dfrac{1}{523}\right)\right]$	
$k_{DME} = 2.51 \times 10^{11} \exp\left[-\dfrac{6.45 \times 10^5}{R}\left(\dfrac{1}{T} - \dfrac{1}{523}\right)\right]$	
$K_{CO} = 4.96 \times 10^{-8} \exp\left[\dfrac{9.93 \times 10^3}{R}\left(\dfrac{1}{T} - \dfrac{1}{523}\right)\right]$	
$K_{CH_3OH} = 1.41 \times 10^{-3} \exp\left[\dfrac{6.05 \times 10^3}{R}\left(\dfrac{1}{T} - \dfrac{1}{523}\right)\right]$	
$K_{CH,CO_2} = 1.43 \times 10^{-4} \exp\left[-\dfrac{2.49 \times 10^3}{R}\left(\dfrac{1}{T} - \dfrac{1}{523}\right)\right]$	Coteron and Hayhurst [11]
$K_{H_2} = 6.37 \exp\left[-\dfrac{6.29 \times 10^3}{R}\left(\dfrac{1}{T} - \dfrac{1}{523}\right)\right]$	
$K_{CH,CO} = 7.12 \exp\left[-\dfrac{3.17 \times 10^3}{R}\left(\dfrac{1}{T} - \dfrac{1}{523}\right)\right]$	
$K_{H_2O} = 2.85 \exp\left[-\dfrac{1.08 \times 10^5}{R}\left(\dfrac{1}{T} - \dfrac{1}{523}\right)\right]$	
$K_{CO_2} = 70.015$	
$K_{H_2O,DME} = 0.84 \times 10^{-1} \exp\left[\dfrac{4.11 \times 10^4}{RT}\right]$	Ng et al. [20]

Mass balance: $u_s \dfrac{dC_i}{dz} = k_g a_v (C_{s,i}^s - C_i)$ (13)

Energy balance: $u_s \rho_g C_P \dfrac{dT}{dz} = h_f a_v (T_s^s - T) - \dfrac{4U}{D_t}(T - T_W)$ (14)

Boundary condition: $c_i = c_{i,0}$ and $T = T_{in}$ at $z = 0$ (15)

ii) For catalyst particle

Mass balance: $\rho_B \eta R_j + k_g a_v (C_i - C_s^s) = 0$ (16)

Energy balance: $\rho_B \sum\limits_{j=1}^{NR} (-\Delta H)_j \eta_j R_j + h_f a_v (T - T_s^s) = 0$ (17)

where c and T represent the concentration and temperature of the fluid phase, respectively, while the symbols with subscript s correspond to the properties in the solid (catalyst) state. Superscript s denotes the values at the surface of the catalyst. More details about the symbols are referred to the 'Nomenclature' section. The values of C_P, ΔH_j, gas density of component i ($\rho_{g,i}$) and thermal conductivity of gas are available in a process simulator (UniSim Design Suite, Honeywell Inc.). The symbol a_v is specified as 0.6257 and the porosity (ε), used in the calculation of catalyst density, is 0.39 [17].

Mass and heat transfer coefficients in m/s and kJ/ m^2·s·K, respectively, are calculated from the following equations [22-24]:

$k_{g,i} = 0.91 N_{Re}^{0.49} N_{Sc}^{1/3} \psi D_{m,i} d_p^{-1}$ (18)

$h_f = 0.91 N_{Re}^{0.49} N_{Pr}^{1/3} \psi k_{mix} d_P^{-1}$ (19)

Effectiveness factors are calculated using the dusty gas model [25,26], in which the mixed diffusion ($D_{m,i}^e$) is determined as follows:

$\dfrac{1}{D_{m,i}^e} = \dfrac{1}{D_{K,i}} + \sum\limits_{\substack{j=1 \\ j \neq i}}^{N} \dfrac{C_j}{D_{i,j} C_t}$ (20)

$D_{K,i} = \dfrac{4}{3} r_{pore} \sqrt{\dfrac{8RT}{\pi M_i}}$ (21)

$D_{i,j} = \dfrac{10^{-4} T^{1.75} (M_i^{-1})^{1/2}}{P_{atm} (\sum v_i^{1/3} + \sum v_j^{1/3})^2}$ (22)

where $D_{K,i}$ and $D_{i,j}$ represent the Knudsen diffusion coefficient for component i in m^2/s and binary diffusion coefficient in m^2/s, respectively, and diffusion volume (v_i) is summarized in Table 3.

After other parameters such as pseudo-equilibrium constants ($K_{eq,i}$) for component i and pseudo first-order reaction rate constants (k_i'') for component i are calculated (cf. refer to Lommerts et al. [25]), the Thiele modulus is determined as follows:

Table 3. Diffusion volume for component i [27]

Components	Diffusion volume (v_i) [cm^3/ mol]	Molecular weight [g/mol]
CH$_3$OH	29.9	32.04
H$_2$O	12.7	18
H$_2$	7.07	2.016
CO	18.9	28.01
CO$_2$	26.9	44.01
CH$_3$OCH$_3$	50.36	46.07

$\phi_{M,i} = \dfrac{r_{pellet}}{3} \sqrt{\dfrac{k_i'''(K_{eq,i}+1)}{D_{m,i}^e K_{eq,i}}}$ (23)

Finally, the effectiveness factor is calculated by using the following equation [28]:

$\eta_i^e = \dfrac{1}{\phi_{M,i}} \dfrac{(3\phi_{M,i}) \coth(3\phi_{M,i}) - 1}{3\phi_{M,i}}$ (24)

3. Model Validation

Kinetic parameters are specified by using the values estimated in our previous work [13], where the synergetic effect of CO$_2$ on the methanol production rate has been proven in a systematic manner. It is worth noting that although the kinetic parameters have been estimated using the data in the lab-scale reactor, the values are not completely intrinsic due to the model mismatch resulting from unknown reactor dynamics and so on. In other words, since the values include some information on reactor dynamics, they may cause a little deviation when applied to a bench-scale reactor. Therefore, the overall heat transfer coefficient (U) and some of the kinetic parameters are modified to fit the experimental data measured in the bench-scale system; thus, the values of k_C and U are re-estimated (cf. Table 2) using the *lsqcurvefit* toolbox in MATLAB (The MathWorks Inc.). The value of U for a bench-scale reactor is decreased from 800 J/ m^2·s·K for a lab-scale reactor to 100 kJ/m^2·s·K, indicating that the heat is poorly transferred in a bench-scale reactor. The value of the pre-exponential factor for kinetic rate constants k_C is determined to be 45 times higher than that in the lab-scale reactor.

Fig. 2 shows a comparison between the simulation results and experimental data. Temperature is measured at five points with the thermocouple installed in the reactor (cf. Fig. 1), and space velocity (GHSV) is specified to be 4,020 L/kg$_{cat}$·h. The gas composition of CO : CO$_2$: H$_2$ is 1 : 0.35 : 2.81, and wall temperature is 458 K, while the pre-heater is set to 483 K in order to initiate the methanol synthesis reaction. It is shown that the temperature profile calculated by the simulation deviates from the measured data, but the CO and CO$_2$ conversions at the exit of the reactor are predicted satisfactorily. Experimental data for the temperature profile shows the behavior
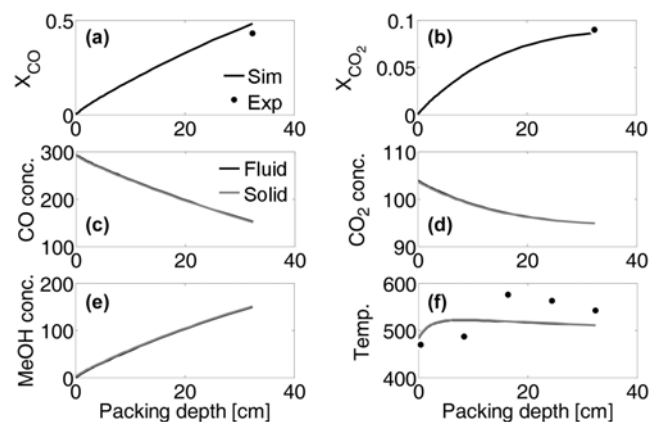

Fig. 2. Comparison of (a) CO conversion and (b) CO$_2$ conversion between experimental data and simulation results for the bench-scale reactor. Diagrams (c) to (f) show the profiles of CO concentration, CO$_2$ concentration, MeOH concentration and temperature, respectively, in the fluid and solid phase.

that the temperature is abruptly increased in the middle of the packing area, which is not consistent with the usual characteristics of fixed-bed reactors, while the simulated results clearly show that the temperature increases from the inlet of the reactor. This feature may be attributed to the measurement error. However, the maximum error at the packing depth of about 16 cm (the third point from the inlet) is less than 9%, and the average error and standard deviation of errors are about 2.7% and 7%, respectively. Therefore, the validity of the model is corroborated. It is worth noting that since the usual operation temperature ranges from 513 to 533 K in low pressure processes [5], a wall temperature of 458 K results in an increase of temperature in the reactor to this range due to the exothermic characteristic of the reaction. Another observation is that the profiles of concentrations as well as reactor temperatures between fluid and solid phase almost coincide, indicating that the mass and heat transfer resistance in the film layer of solid catalyst particle is almost negligible.

OPTIMIZATION AND RESULTS

1. Optimization Strategies

In the optimization step, several cases are suggested to evaluate their performance for the maximization of methanol production rate. Case 1 considers the feed temperature and the wall temperature as manipulated variables, while Case 2 manipulates the feed temperature and assumes that the reactor is composed of three sub-sections to which a different wall temperature is applied. In Case 3, the effect of CO_2 fraction on the methanol yield is investigated, compared to the other manipulated variables, that is, the feed and the wall temperatures. It should be noted that, to our knowledge, no research work has applied the optimal CO_2 fraction in order to consider the synergetic effect by the addition of carbon dioxide, although several attempts have been made to maximize the methanol synthesis reaction rate using optimization strategies for the temperature profile.

As shown in Fig. 3, the optimal CO_2 fraction for maximum methanol yield is dependent on the reaction temperature in the isothermal reactor. T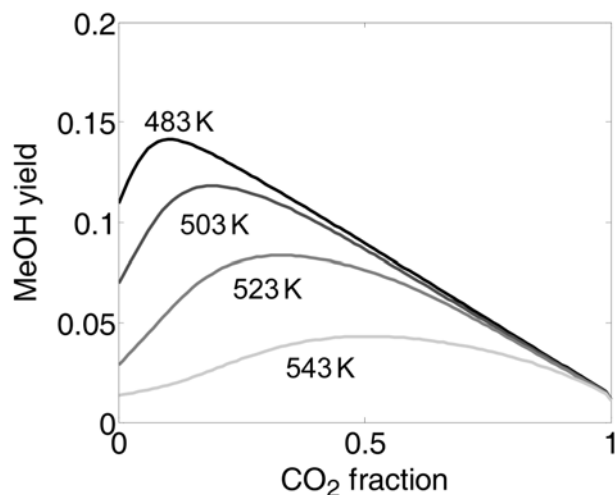his feature suggests that, considering the variation of reaction temperature within the reactor, it might be beneficial if one can take the profile of CO_2 fraction into account as manipulate variable. For this purpose, the application of a piece-wise profile of the CO_2 fraction, utilizing the additional feed at the inlet of the second and the third sections, is included in Case 4.

For all cases, the upper constraints on the feed and wall temperatures are specified as 523 K since a temperature in the reactor higher than 543 K causes the deactivation of catalyst pellets [15], while the lower constraint of 423 K guarantees the activation of catalyst for MeOH synthesis as reported in the literature [5].

2. Genetic Algorithms

The objective function, composed of methanol production rate, is maximized by using the *Genetic Algorithm* toolbox in Matlab (The MathWorks Inc.). Genetic algorithm (GA) is a class of probabilistic optimization algorithms inspired by the biological evolution process. GA maintains a population of candidate solutions (called chromosomes) for the problem at hand and makes it evolve by iteratively applying a set of stochastic operators summarized as follows [17,29]:

• Selection rules select the individuals, called parents, that contribute to the population at the next generation.
• Crossover rules combine two parents to form children for the next generation.
• Mutation rules apply random changes to individual parents to form children.

3. Results and Discussion

It should be noted that, in the optimization step, a one-dimensional pseudo-homogeneous plug flow reactor model is used to simulate the reactor in order to reduce the computational load. The utilization of the pseudo-homogeneous model is also justified by little difference in the profiles of temperature as well as concentrations between fluid phase and solid state as shown in Fig. 2. The specification of optional variables in the GA toolbox is provided in Table 4.

Table 4. Options specified in Genetic Algorithm toolbox

Number of decision variables	3-9
Population size	20
Population type	Double vector
Tolerance	1e-10
Stall time limit	4800
Stall gen limit	80
Generation number	100-300
Mutation function mutation rate	Uniform 0.01

Table 5. Comparison of optimization strategies and the corresponding result

Case	Manipulated variables	MeOH yield [gmol/s·m²]	Scaled yield[a]	Remarks
Case 1	T_{in}, $T_{w, 1}$	0.1126		Fig. 4
Case 2	T_{in}, $T_{w, i}$	0.1247		Fig. 5
Case 3	T_{in}, $T_{w, i}$, $y_{CO2, 1}$	0.1952	0.4268	Fig. 6
Case 4	T_{in}, $T_{w, i}$, $y_{CO2, i}$	0.2564	0.4218	Fig. 7

[a]MeOH yield divided by the total amount of CO and CO_2 fed to the reactor

Fig. 3. Effect of CO_2 fraction on the MeOH yield under a variety of reaction temperatures. Isothermal operation is assumed for the calculation.
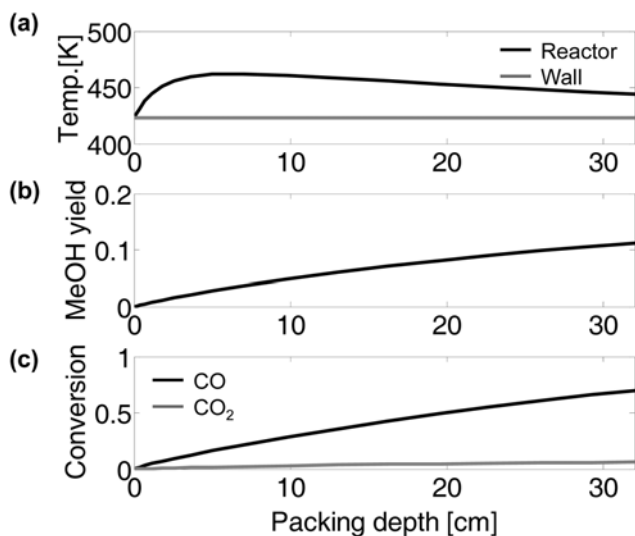
Fig. 4. Optimization results for the Case 1. (a) Reactor and wall temperatures, (b) methanol yield, (c) CO and CO_2 conversions.

Details about the optimization strategy for each case and their corresponding results are summarized and compared in Table 5. The results of Case 1 show the effect of wall temperature on the MeOH yield, when the CO_2 fraction is fixed at 0.5 (cf. Fig. 4). Since the reaction is reversible and exothermic, a low temperature makes the MeOH yield at the exit of the reactor increase, compared to the operation under high reaction temperature. This feature is also reported in the literature [15], and thus, Case 1 infers that the reaction temperature should be kept to be as low as possible if the deactivation of catalyst is insignificant.

Although a low temperature results in high equilibrium conversion, it is less effective in the sense of reaction rate. Considering that the operation in the bench-scale reactor in the present study
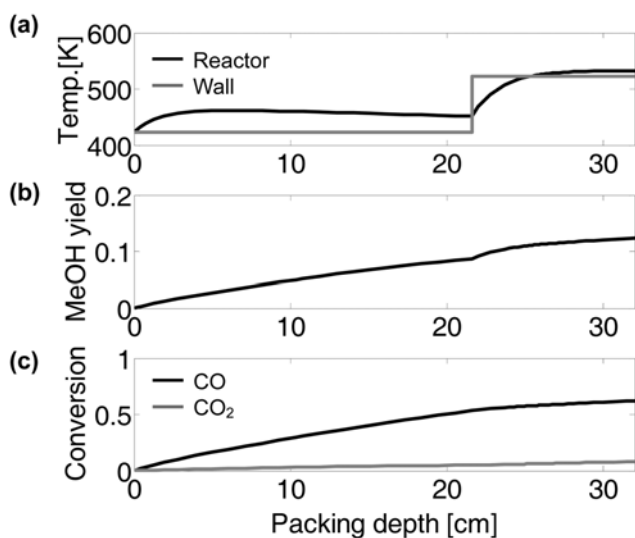

Fig. 5. Optimization results for the Case 2. (a) Reactor and wall temperatures, (b) methanol yield, (c) CO and CO_2 conversions.
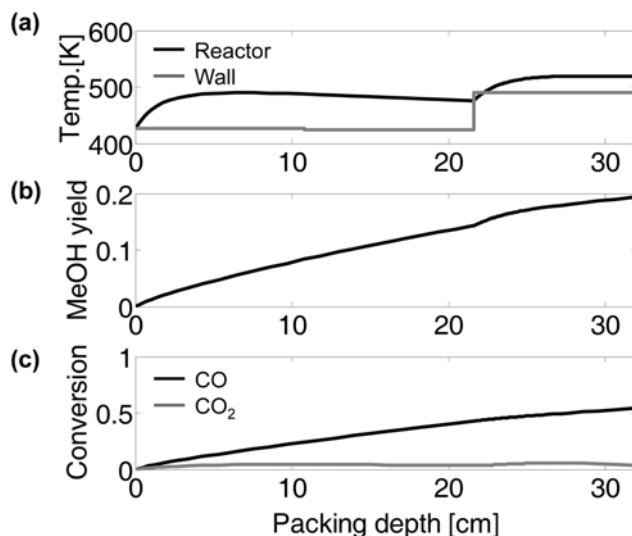
does not completely reach equilibrium (cf. Fig. 2), it might be useful to apply the temperature trajectory in order to maximize both the reaction rate in the reactor and the conversion at the exit. For this purpose, a piece-wise trajectory is assumed for the temperature, and thus, the reactor is assumed to be divided into three sections. Fig. 5 shows the optimization results when the inlet temperature and wall temperatures in each section are specified as manipulated variables. The inlet temperature and wall temperatures in the first two sections are optimized to be lower bound, but the third section is operated at the temperature of upper bound. As a result, the MeOH yield is increased (0.1247 gmol/m²·s for Case 2) further than the case of low temperature for whole sections (0.1126 gmol/m²·s for Case 1). This feature may be attributed to the higher consumption rate of CO_2 than that of carbon monoxide in this operating region, as observed in the increased CO_2 conversion in the third section while CO conversion in the section is decreased.

In Case 3, the CO_2 fraction is included in the set of manipulated variables, and the results are provided in Fig. 6. The optimal value for CO_2 fraction is determined by GA to be 7.08%, which is close to the optimal value for the operation under isothermal condition of 483 K (cf. Fig. 3). This is because most of the reaction takes place in the earlier part of the reactor, that is, the first two sections where the wall temperatures are maintained at the lower bound and the corresponding reaction temperature is lower than 490 K. The profile of wall temperatures is a little bit different from Case 2. The inlet temperature and the wall temperature in the first section are increased a little bit, while the wall temperature in the third section is lower than Case 2. However, the optimizer still utilizes the phenomenon that the CO_2 consumption rate in this region is higher than the CO hydrogenation rate. It is observed in Fig. 6(c) that CO conversion is decreased, compared to the previous cases, since the amount of CO is increased. However, the production rate of methanol (MeOH yield in Fig. 6(b)) is high because the CO hydrogenation rate is higher than CO_2 hydrogenation [13] and an optimal amount of CO_2 leads to the synergetic effect on methanol synthesis.

Fig. 6. Optimization results for the Case 3. (a) Reactor and wall temperatures, (b) methanol yield, (c) CO and CO_2 conversions.
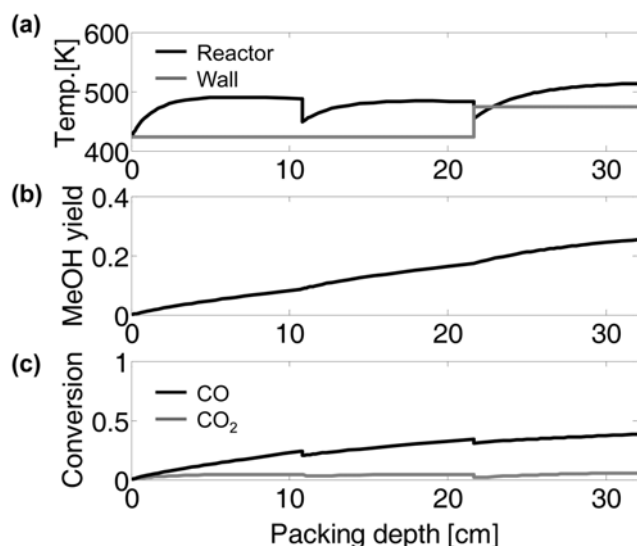
Fig. 7. Optimization results for the Case 4. (a) Reactor and wall temperatures, (b) methanol yield, (c) CO and CO_2 conversions.

Since it is observed that the reaction temperatures in each section are different, Case 4 applies the trajectory for CO_2 fraction in the reactor, which is approximated by a piece-wise trajectory. The CO_2 fraction in each section is manipulated by two additional feeds between each section while the total amount of additional feed at each section is fixed at 30% of the feed at the inlet of the reactor. CO_2 fractions at the inlets of each section are determined to be 2.44%, 0.71%, and 10.44%, respectively. The resulting trajectory, which is provided in Fig. 7, indicates that CO is mostly consumed for the synthesis of methanol in the first two sections, while more CO_2 is used in the third section because the reaction temperature is higher than that in the other sections and the optimal CO_2 fraction for high temperature is higher than that for low temperature. As the feeds are additionally fed to the reactor, the MeOH yield (0.2564 gmol/$m^2 \cdot s$) is much more increased than Cases 1-3. To clearly compare the efficiencies of Cases 3 and 4, the MeOH yield is divided by the whole amount of CO and CO_2 fed to the reactor (named as 'scaled yield'), and the values for Cases 3 and 4 are 0.4268 and 0.4218, respectively. However, if the amount of hydrogen feed is considered in the calculation of the scaled yield, Case 4 is no longer found to be efficient. In addition, the application of the additional feed results in an increase in the capital investment, and thus, the effectiveness of Case 4 is further decreased. This feature is attributed to the fact that the third section plays a less important role in the production rate than the other sections because of the characteristics of the packed-bed reactor, and the residence time of additional feeds is lower than the inlet feed, resulting in the decrease in the production rate. Although the reaction rate is a little bit increased since the cold additional feed decreases the reaction temperature at the inlets of the second and the third sections, this does not compensate for the inefficiency of Case 4 discussed above.

If the amount of additional feed is also considered as an argument in the optimization strategy, the optimal values are determined to be zero, indicating that the additional feed lessens the efficiency of the process. Therefore, it is shown that the application of an op-

timal temperature profile and optimal CO_2 fraction at the inlet is the best strategy, given the methanol production efficiency and the capital investment.

CONCLUSIONS

A mathematical model of the bench-scale reactor for the synthesis of methanol over $Cu/ZnO/Al_2O_3/ZrO_2$ catalyst is developed, and its validity is corroborated by comparing the simulation results with experimental data. Since the kinetics model clearly considers the effect of carbon dioxide on the methanol production rate as a function of temperature, the optimization strategy is suggested by applying the optimal CO_2 fraction. The comparison of the optimization results with other cases shows that the methanol yield per unit amount of feed is significantly increased due to the optimized CO_2 fraction as well as the optimal temperature profile in the reactor. In conclusion, the strategy suggested in this study can be effectively applied to the determination of optimal operating conditions in industrial methanol synthesis processes.

ACKNOWLEDGEMENTS

NOMENCLATURE

C_A : concentration [mol/cm³]
C_p : heat capacity [kJ/kg/K]
C_{WP} : weisz-prater parameter
D : tube diameter [m]
D^e : effective diffusivity [m²/s]
$D^e_{i,j}$: binary diffusion coefficient for component i and j [cm²/s]
D^e_{Ki} : knudsen diffusion coefficient [cm²/s]
$D_{m,i}$: mixed effective diffusion coefficient [m²/s]
D_t : tube diameter [m]
d_p : paticle diameter [m]
E : activation energy [kJ/kmol]
F_{obj} : objective function
H_j : reaction enthalpy [kJ/mol]
h_f : gas-solid heat transfer coefficient [J/m²/s/K]
K_i : species adsorption equilibrium constants
$K_{P,1}$: reaction equilibrium constants
k_g : mass transfer coefficient for component i
k_l : forward reaction rate constant (l=A, B, C, DME), [gmol/g_{cat}/s]
k_{mix} : gas phase thermal conductivity [kJ/s/m/K]
M_i : molecular weight [g/gmol]
N : total number of data point

N_{Pr} : prandtl number
N_{Re} : reynolds number
N_{Sc} : schmidt number
n : reaction order
P_{atm} : atmosphere pressure
P_i : pressure [Pa]
R : gas constant (R=8.314) [J/gmol/k]
R_j : reaction rate [mol/kg$_{cat}$/s]
$r_{A, obs}$: observed rate [mol/kg$_{cat}$/s]
r_1 : reaction rate [mol/kg$_{cat}$/s]
r_{pellet} : pellet diameter [m]
T : temperature [K]
T_s^s : temperature of solid phase [K]
T_w : wall temperature [K]
U : overall heat transfer coefficient [J/m²/s/K]
u_s : linear velocity [m/s]
V_s : space volume
V_t : total volume
V_v : vacancy colume
v_i : diffusion volume [cm³/mol]
X : conversion
y_i : fraction for component i
z : packing depth [m]

Greek Letters

α_v : specific surface area of catalyst pellet [m²/m³]
ε_B : void fraction of catalyst bed
ϕ_M : thiele modulus
η : effectiveness factor
ρ_c : solid catalyst density [kg/m³]
ρ_B : bulk pellet densities [kg/m³]
ρ_g : gas densities [kg/m³]
ψ : shape factor in the mass-transfer coefficient equation [Particle=1]

REFERENCES

1. G. A. Olah, H. Doggweiler, J. D. Felberg, S. Frohlich, M. J. Grdina, R. Karpeles, T. Keumi, S. Inaba, W. M. Ip, K. Lammerstsmak, G. Salem and D. C. Tabor, *J. Am. Chem. Soc.*, **106**, 2143 (1984).
2. G. A. Olah, *Angew. Chem. Int. Ed.*, **44**, 2636 (2005).
3. G. K. S. Prakash, M. C. Smart, Q.-J. Wang, A. Atti, V. Pleynet, B. Yang, K. McGrath, G. A. Olah, S. R. Narayanan, W. Chun, T. Valdez and S. Surampudi, *J. Fluorine Chem.*, **125**, 1217 (2004).
4. J. P. Lange, *Catal. Today*, **64**, 3 (2001).
5. C. N. Satterfield, *Heterogeneous catalysis in industrial practice*, McGraw-Hill, New York (1991).
6. R. G. Herman, K. Klier, G. W. Simmons, B. P. Finn and J. B. Bulko, *J. Catal.*, **56**, 407 (1979).
7. G. C. Chinchen, P. S. Denny, D. G. Parger, M. S. Spenser and D. A. Whan, *Appl. Catal.*, **30**, 333 (1987).
8. B. Denise and R. P. A. Sneeden, *J. Mol. Catal.*, **17**, 359 (1982).
9. K. Klier, V. Chatikavanij, R. G. Herman and G. W. Simmons, *J. Catal.*, **74**, 343 (1982).
10. J. F. Edwards and G. L. Schrader, *J. Phys. Chem.*, **88**, 5624 (1984).
11. A. Coteron and A. N. Hayhurst, *Chem. Eng. Sci.*, **49**, 209 (1994).
12. M. A. McNeil, C. J. Schack and R. G. Rinker, *Appl. Catal.*, **50**, 265 (1989).
13. H.-W. Lim, M.-J. Park, S.-H. Kang, H.-J. Chae, J. W. Bae and K.-W. Jun, *Ind. Eng. Chem. Res.*, **48**, 10448 (2009).
14. I. Løvik, M. Hillestad and T. Hertzberg, *Comput. Chem. Eng.*, **22**, S707 (1998).
15. H. Kordabadi and A. Jahanmiri, *Chem. Eng. J.*, **108**, 249 (2005).
16. M. R. Rahimpour and M. Lotfinejad, *Chem. Eng. Technol.*, **30**, 1062 (2007).
17. M. R. Rahimpour and H. Elekaei Behjatia, *Fuel Process. Technol.*, **90**, 279 (2009).
18. G. H. Graaf, P. J. J. M. Sijtsema, E. J. Stamhuis and G. E. H. Joosten, *Chem. Eng. Sci.*, **41**, 2883 (1986).
19. P. Mizsey, E. Newson, T. Truong and P. Hottinger, *Appl. Catal. A: Gen.*, **213**, 233 (2001).
20. K. L. Ng, D. Chadwick and B. A. Toseland, *Chem. Eng. Sci.*, **54**, 3587 (1999).
21. H. Kordabadi and A. Jahanmiri, *Chem. Eng. Process.*, **46**, 1299 (2007).
22. H. J. Chae, S. T. Choo, H. I. Choi and S. Nam, *Ind. Eng. Chem. Res.*, **39**, 1159 (2000).
23. T. H. Chilton and A. P. Colburn, *Ind. Eng. Chem.*, **26**, 1183 (1934).
24. R. H. Perry and D. W. Green, *Perry's Chemical Engineers' Handbook*, McGraw-Hill, New York (1997).
25. B. J. Lommerts, G. H. Graaf and A. A. C. M. Beenackers, *Chem. Eng. Sci.*, **55**, 5589 (2000).
26. R. Suwanwarangkul, E. Croiset, M. W. Fowler, P. L. Douglas, E. Entchev and M. A. Douglas, *J. Power Sources*, **122**, 9 (2003).
27. E. N. Fuller, P. D. Schettler and J. C. Gidding, *Ind. Eng. Chem.*, **58**, 19 (1966).
28. K. R. Westerterp, W. P. M. Van Swaaij and A. A. C. M. Beenackers, *Chemical reactor design and operation*, Wiley, Chichester (1987).
29. D. E. Goldberg, *Genetic Algorithms in Search, Optimization, and Machine Learning*, Addison-Wesley, Reading (1989).